Growth of C_{60} thin films on GeS(001) studied by scanning force microscopy

U. D. Schwarz and W. Allers
Institute of Applied Physics, University of Hamburg, Jungiusstrasse 11, D-20355 Hamburg, Germany

G. Gensterblum and J.-J. Pireaux
Laboratoire Interdisciplinaire de Spectroscopie Electronique, Facultés Universitaires Notre-Dame de la Paix, 61, rue de Bruxelles, B-5000 Namur, Belgium

R. Wiesendanger
Institute of Applied Physics, University of Hamburg, Jungiusstrasse 11, D-20355 Hamburg, Germany
(Received 16 February 1995)

The epitaxial growth of C_{60} thin films sublimed onto GeS(001) substrates under ultrahigh-vacuum conditions was investigated in the range of 0.7–11 monolayers coverage by scanning force microscopy in air. The growth process follows basically a layer-by-layer mechanism if evaporated in the narrow temperature range from 180 to 200 °C, but was found to be very sensitive to even small changes in temperature. At substrate temperatures above 200 °C, the second and higher layers are not stable. For temperatures close to 200 °C, our studies indicate pure layer-by-layer-type growth. Somewhat lower substrate temperatures lead to the formation of two different types of triangular-shaped islands which originate from a different stacking of the molecules, beginning with the second layer. Triangular islands belonging to the same type tend to coalesce, whereas islands of different types are separated by grooves. At substrate temperatures close to 180 °C during evaporation, dendritic islands are formed due to the limited mobility of the C_{60} molecules at this temperature. Furthermore, the growth mode changes to a nonideal layer-by-layer growth where the second and even higher layers start to grow before the first layer has been completed. This behavior can well be explained by a two-dimensional diffusion-limited growth mechanism. Finally, substrate temperatures significantly lower than 180 °C result in films without long-range order.

I. INTRODUCTION

During recent years, solid C_{60} has attracted considerable interest in solid-state physics, due to the spherical shape of the C_{60} molecules[1] and the extraordinary properties of the bulk material. With the invention of a method for the production of macroscopic quantities of C_{60},[2] it has become possible to investigate the structural, vibrational, frictional, and electronic properties of this form of carbon. For detailed studies of the solid-state properties of C_{60}, the availability of millimeter-sized C_{60} single crystals[3,4] and high-quality single-crystalline thin films is mandatory. In addition, the growth of C_{60} single crystals and thin films is of fundamental interest, because the individual C_{60} molecules are bound only by the weak van der Waals interaction similar to noble-gas crystals and can adequately be approximated by a hard-sphere model. Therefore, the growth of thin films has been extensively studied on various types of substrates, as, e.g., on metals,[5–8] semiconductors,[9–12] ionic crystals[13–15] and layered materials.[14,16,17] On most substrates, however, the C_{60} thin films were found to grow irregularly or in the Volmer-Weber growth mode (island growth). A more detailed discussion about the growth mechanisms on several different substrates can be found in Ref. 18. One of the rare substrates where layer-by-layer growth of single-crystalline films has been reported is GeS(001).[18,19]

In this paper, we present results of a scanning force microscopy (SFM) study of the growth behavior of C_{60} molecules sublimed in ultrahigh vacuum (UHV) onto single-crystalline GeS(001) substrates. The surface morphology measurements have been combined with simultaneous lateral force measurements. This additional data allows us to make a clear distinction between substrate and C_{60} layers, i.e., enabling chemical contrast[20] and thereby facilitating the image interpretation. Moreover, it provides information about the microtribological properties of the C_{60} layers, which are still considered as a solid lubricant despite contradictory results presented in recent reports.[15,21–26]

II. EXPERIMENT

The sample preparation was carried out under UHV conditions. The single-crystalline, undoped GeS samples of 6 mm × 6 mm × $\frac{1}{2}$ mm size were freshly cleaved *in situ* along their (001) plane. The quality of the cleavage planes was checked by low-energy electron diffraction (LEED), always showing the expected sharp, orthogonally arranged reflections.[18,27] For the evaporation, chromatographically purified C_{60} powder with a purity higher than 99.9% was loaded into the graphite crucible of a Knudsen cell and carefully outgassed at 380 °C for several hours and at 420 °C for 1 h. Finally, the C_{60} molecules were sublimed at 420 °C by opening a shutter for about 3–60 min, depending on the desired film thickness. During the evaporation, the GeS substrate was held at a constant temperature between 180 °C and 200 °C. Sub-

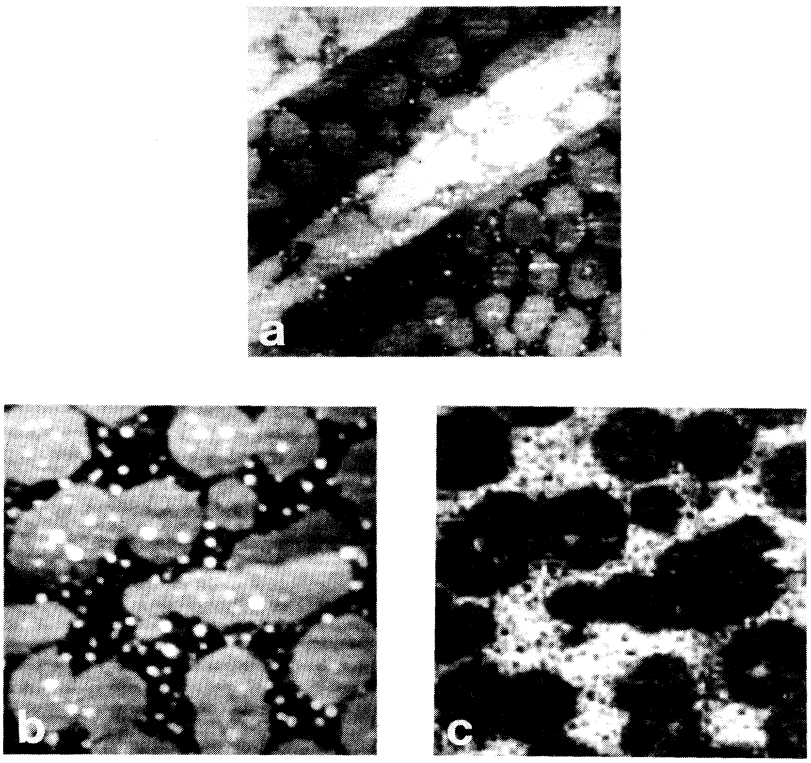

FIG. 1. (a) Force micrograph of a 0.7-ML film. The scanned area was $9.3 \times 9.3\ \mu m^2$. The observed islands are 1 nm high, corresponding to 1-ML C_{60}. The average diameter of an island is around 1 μm. (b) Topography and (c) lateral force map of a smaller surface area on the same film ($4 \times 4\ \mu m^2$). The contrast in the lateral force map indicates lower friction on the C_{60} islands.

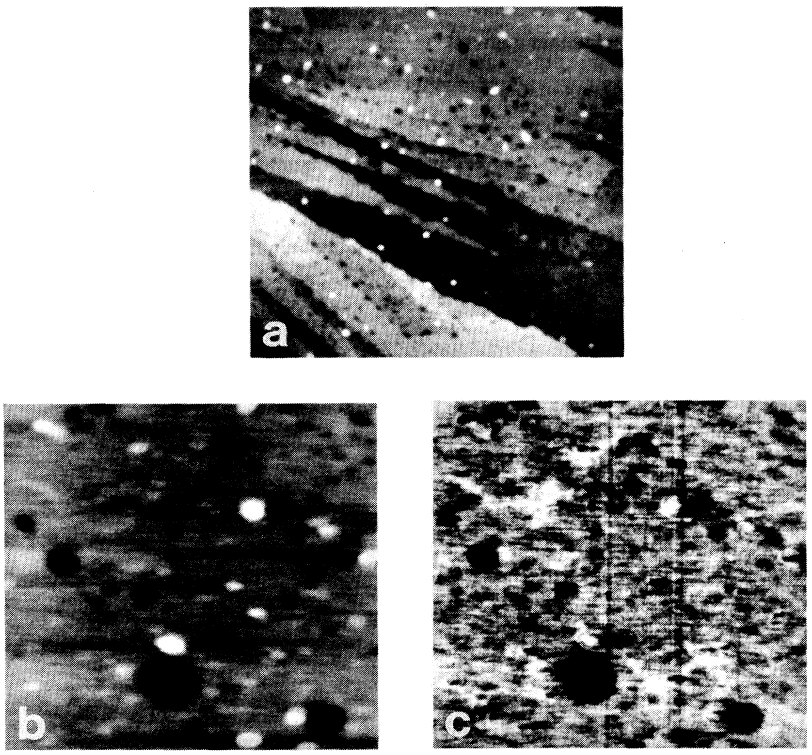

FIG. 2. (a) Large-scale scan ($12.5 \times 12.5\ \mu m^2$) of a 0.95-ML film. Small holes are observed. The step structure is induced by the cleavage steps of the underlying substrate. (b) Zoom of (a) for a closer examination of the holes. These holes are found to be 1-nm deep and flat at the bottom. The corresponding lateral force image (c) exhibits a different friction at the bottom of the holes compared with the surface of the film. The reversed contrast [cf. Fig. 1(c)] is explained in the text.

strate heating, which was performed indirectly by using an infrared light source, was started about 10 min before evaporation.

The evaporation rate was determined to be about 0.07 ML/min for the samples presented in Figs. 1–3. For the samples shown in Figs. 4 and 5, a home-built cell was used. The evaporation rate for this cell, estimated from the SFM and LEED investigations, is about three times higher. The background pressure during deposition was $\approx 2\times 10^{-9}$ mbar for all samples. After deposition, the samples were inspected by LEED, revealing diffraction patterns of both GeS and C_{60} with intensities according to the deposition time.[18,27]

Figure 6 shows the structural model for C_{60} molecules on GeS(001) substrates as determined in earlier work.[18,19,27] GeS is a layered material which can easily be cleaved along its (001) plane. Due to the large ionic radius of the sulfur atoms in contrast to the germanium atoms and an anisotropy of the a and b axis of the GeS, rows with 4.4-Å spacing are formed at the surface parallel to the b axis of the substrate (c.f., the side view in Fig. 6). Bulk-C_{60} crystallizes in face-centered cubic (fcc)

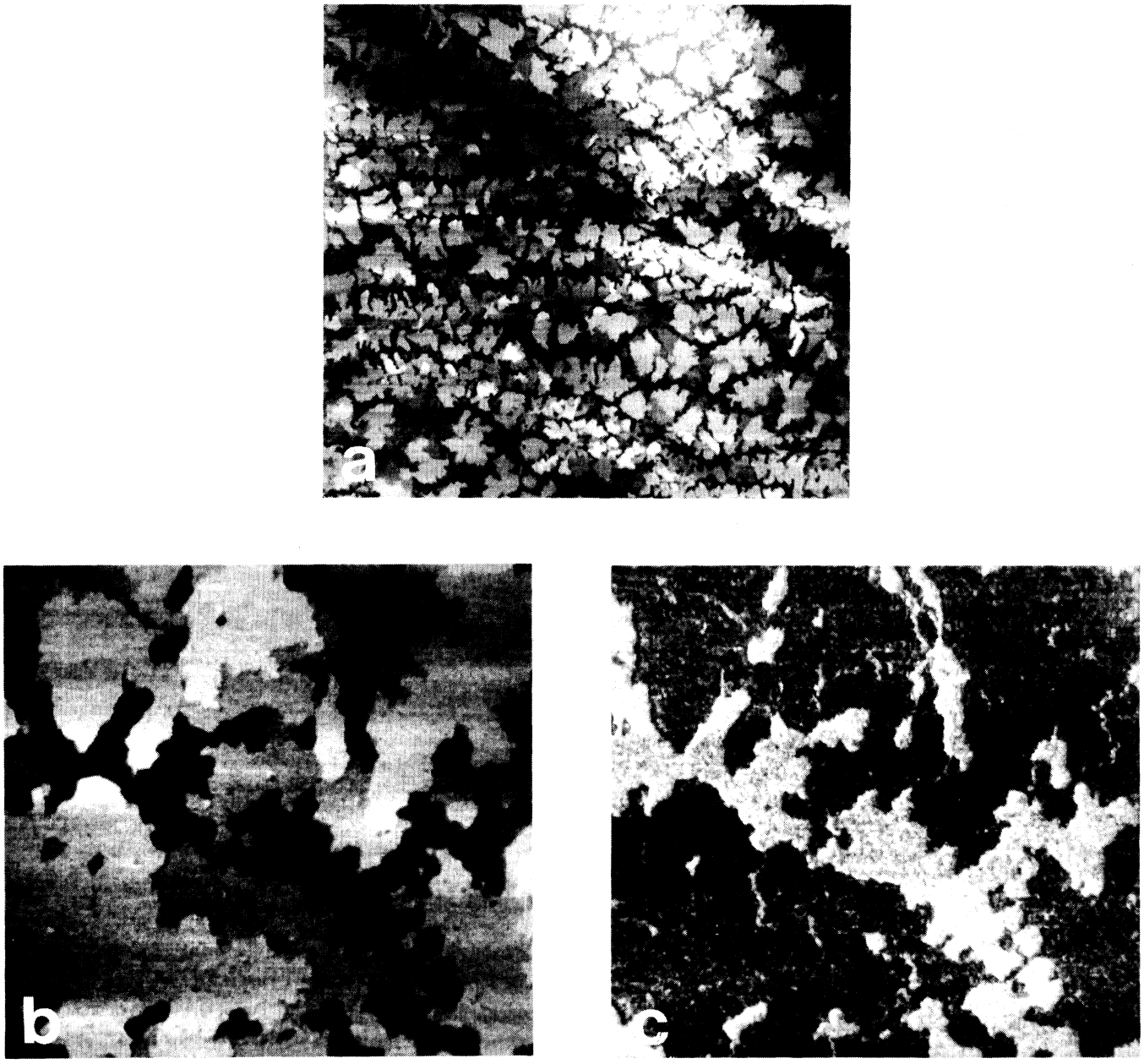

FIG. 3. Large-scale scan [(a) $10\times 10\ \mu m^2$] and higher magnification image [(b) $1.5\times 1.5\ \mu m^2$] of a film with 1.2-ML nominal coverage. The individual islands have about the same diameter as the islands in Fig. 1, but exhibit a dendritic shape. Second and even third monolayer growth starts before the first monolayer has been completed. The individual monolayers are well resolved. (c) Lateral force map of the surface area displayed in (b). The clear contrast allows an easy distinction between substrate and C_{60} layers.

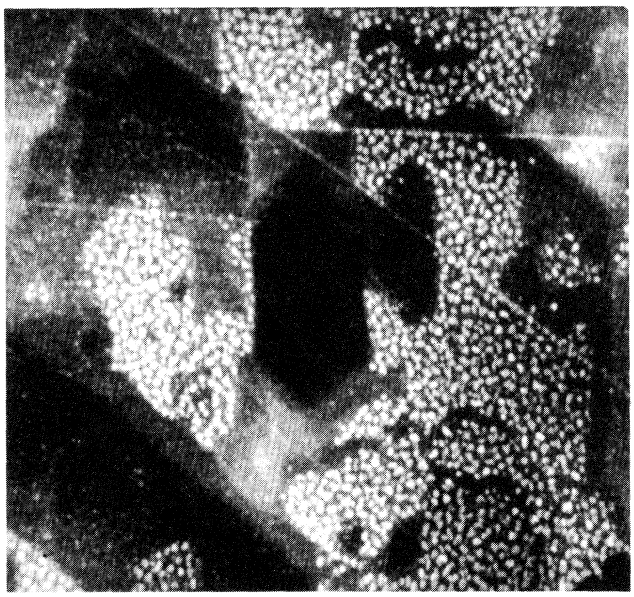

FIG. 4. SFM micrograph (5×5 μm^2) of a sample with $\approx$2-ML coverage. The corresponding lateral force map showed no contrast, indicating that the whole substrate is covered with at least one layer of C_{60}.

structure with a nearest-neighbor distance of 10.02 Å. If the C_{60} molecules fill every second row at the GeS surface, their nearest-neighbor distance matches nearly exactly the bulk value and the C_{60} molecules form a (111) oriented epitaxial layer of a close-packed structure with orientational relations as indicated in Fig. 6.

The scanning force microscopy investigation was performed in air and at room temperature, using a commercially available instrument[28] based on the laser beam deflection method.[29,30] In this setup, normal and lateral forces can be measured in parallel by the simultaneous detection of the vertical and torsional deflection of the cantilever using a four-segment photodiode sensor.[31,32] *V*-shaped Si_3N_4 cantilevers[28] with spring constants of 0.12 N/m were used for the acquisition of the data presented in Figs. 7, 1, and 2 and rectangular silicon cantilevers[33] with spring constants of 0.04–0.15 N/m for all other measurements.

III. RESULTS

For a comparison of covered with uncovered samples, the morphology of freshly cleaved GeS(001) was first characterized by SFM. Figure 7 shows a typical force micrograph of this material; the scanned area is 50×50 μm.[2] Very large, atomically flat terraces are visible, which are separated by steps of 5.3 ± 0.5 Å height or multiples of this value, which is in good agreement with half of the *c*-axis lattice constant of 10.47 Å.[34] Generally, the surface morphology of the freshly cleaved GeS(001) looks similar to the surface morphology of many other layered materials, e.g., graphite.

Figure 1(a) shows the sample after C_{60} molecules have been evaporated on the GeS crystal to form a layer of 0.7-ML nominal thickness. The mapped area is 9.3×9.3 μm^2. Three straight surface steps of about 10-Å height (corresponding to the *c*-axis lattice constant) are visible. Round islands of 10 Å height and 0.5–1.3-μm diameter have been formed. Close to the steps, however, the islands are more longish and oriented along the step direction.

Figure 1(b) shows an SFM micrograph of the same sample at a higher magnification (displayed surface area:

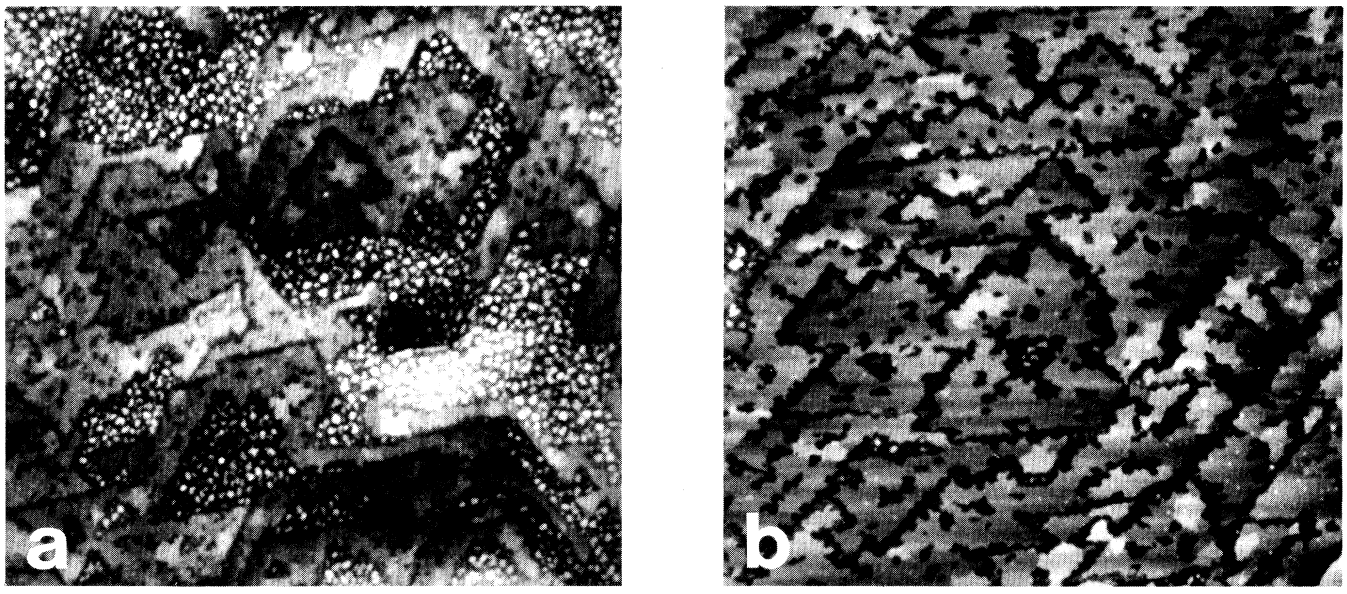

FIG. 5. Force micrographs of two different surface areas on a sample with about 11-ML coverage. The scanned areas are (a) 5×5 μm^2 and (b) 3.6×3.6 μm^2. The triangular-shaped islands, reflecting the sixfold symmetry of the $C_{60}\{111\}$ surface, are separated by grooves of 1-ML depth and 50–140-nm width. A mechanism which could explain the observed surface structure is proposed in the discussion.

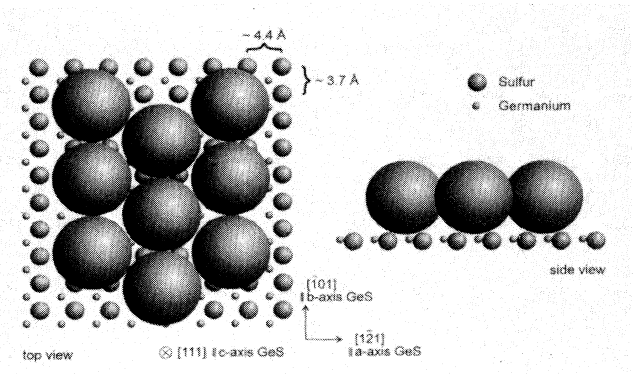

FIG. 6. Structural model for C_{60} molecules on GeS(001). Due to the anisotropy of the *a* and *b* axes of the GeS crystal and the different radii of the sulfur and the germanium ions, parallel rows in the *b* direction with 4.4-Å distance are formed on the GeS(001) surface. This is nearly half of the interlayer distance of two {111} layers in the C_{60} bulk crystal. If every second row is filled, the nearest-neighbor distance of two C_{60} molecules fits well to the 10.02-Å bulk value. Therefore, large grains with low internal stress can be formed.

4×4 μm^2). Several islands already started to coalesce. The upper part of the image is about 5 Å lower than the lower part, due to a cleavage step of the substrate crossing the image in the middle. Figure 1(c) shows a simultaneously recorded lateral force map of the same surface spot; dark means low and bright means high lateral force in this image. The contrast in the lateral forces demonstrates that the islands consist of another material than the substrate and thus allows us to make a clear distinction between substrate and C_{60} layers, as shown in Ref. 19. By comparing the measured height of the islands of 10 Å with the nearest-neighbor distance of the individual C_{60} molecules in the bulk of 10.02 Å, the islands can be identified as C_{60} islands of 1-ML height. Second C_{60} layer growth was not observed on this sample on any surface area investigated. The white spots in the topography images of the sample are clusters, most likely consisting of an assembly of C_{60} molecules. These clusters, exhibiting heights of 1–4 nm, were equally distributed on the sample at the beginning of the measurement, but wiped away during scanning from the top of the C_{60} islands. In the lateral force map, the black spikes in the white-colored GeS substrate area are due to a topography-induced component of the lateral force signal, which is proportional to the slope of the surface, and is caused by the clusters.[35,36] Similar white features are also visible on the black C_{60} island at the positions of larger clusters in the topography image.

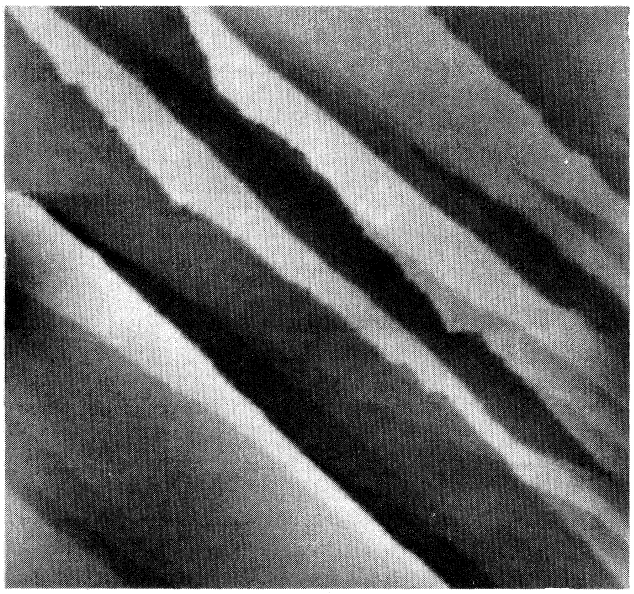

FIG. 7. SFM micrograph of freshly cleaved GeS(001). The image is dominated by large, atomically flat terraces, which are separated by steps of half of the *c*-axis lattice-constant height (5.3 Å) and multiples of this value. The scanned surface area is 50×50 μm^2.

Figure 2(a) shows a 12.5×12.5 μm^2 area on a 0.95-ML sample. Larger terraces with small holes are observed. The white spots are again clusters, but, compared with the sample presented in Fig. 1, with a much lower density. Higher magnification micrographs as, e.g., the images displayed in Figs. 2(b) and 2(c) [(b) topography, (c) lateral force map, scanned area: 3×3 μm^2] were taken to study the holes in more detail. They were found to be 10-Å deep and flat at the bottom. The height corresponds again to 1 ML, but can also be explained by a step of one unit cell of the GeS substrate. The bottom of the holes, however, always showed a significantly different contrast in the lateral force image than the rest of the scanned area. Hence it follows that the sample surface is covered with a single, nearly continuous monolayer of C_{60} molecules. Except for structures induced by cleavage steps of the substrate, no grain structure or additional texture was observed.

In Fig. 3, force micrographs of a 1.2-ML C_{60} film are presented. This sample was free of clusters and exhibited a low adhesion of about 6–7 nN when scanned with silicon tips. Therefore, it was an ideal specimen for exact quantitative measurements for both topographical and lateral force issues. Figure 3(a) shows a large-scale scan (10×10 μm^2), Figs. 3(b) and 3(c) topography and lateral force map of a smaller surface area (1.5×1.5 μm^2). The individual islands have about the same diameter compared with the 0.7-ML film, but are of dendritic shape. The clear contrast in the lateral force map [Fig. 3(c)] and the molecular resolution, which was obtained on the C_{60} overlayer,[19] confirmed that the islands are formed by C_{60} molecules. The GeS substrate, however, is still visible. In contrast to the 0.7- and 0.95-ML film, second and even third-layer growth has been observed. The lateral force image shows no contrast between the first and the second or third layer, demonstrating that the different terraces consist of the same material. A statistical analysis revealed that about 30% of the substrate is not covered, but $\approx40\%$ of the substrate is covered with at least two C_{60} layers and $\approx4\%$ with even three layers. By means of averaging, the step height between the substrate and the

first layer was determined to be 10.5±1 Å, which is in agreement with the nearest-neighbor distance in the C_{60} crystal, as already discussed above, and with the step heights measured for the samples presented in Figs. 1 and 2. The step heights between the first and the second as well as the second and the third layer, however, are 8.4±1 Å. This value corresponds nearly perfectly to the theoretical step height of 8.2 Å between {111} planes in a C_{60} fcc lattice with 10.02-Å nearest-neighbor distance.

Additionally, a quantitative analysis of the lateral forces was performed for this sample. In Fig. 3(c), bright color represents high and dark color low lateral force; hence the friction on the C_{60} islands is obviously significantly reduced in comparison to the GeS substrate. The loading force F_n of the cantilever in this image was 10 nN. From a series of data obtained between 1- and 20-nN loading force, the ratio between the friction coefficient on C_{60} monolayers, $\mu_{C_{60}}$, and the friction coefficient on the GeS substrate, μ_{GeS}, was determined to be $\mu_{C_{60}}$: $\mu_{GeS} \approx 2{:}3$. The individual friction coefficients $\mu = F_l/F_n$ (where F_l denotes the lateral force) were determined by a straight-line model allowing an offset. A closer analysis, however, shows that such a simple model is probably not appropriate. Between 7 and 10 nN loading force, the contrast flips in the lateral force images. Below $F_l \approx 7$ nN, the lateral force on the C_{60} molecules is *higher* than on the GeS substrate [see, e.g., Fig. 2(c), which was imaged with low loading force and shows reversed contrast in comparison with Figs. 1(c) and 3(c)]; measurements above $F_l \approx 10$ nN always exhibited *lower* lateral forces on the C_{60} layers than on the substrate. This effect can be explained by a different dependence of F_l on F_n for the C_{60} layers compared with the GeS substrate. A detailed discussion of these issues is given elsewhere.[37]

Furthermore, the absolute values for the friction coefficients varied in quite a wide range. In several independent measurements on freshly cleaved GeS, e.g., numerical values from 0.24 up to 1.53 were found for μ_{GeS}, in spite of the fact that extreme care had been taken to obtain a correct calibration of the lateral forces. This variation might be influenced by the shape of the profiling tip, i.e., the actual contact area, and perhaps also by other parameters like the humidity or the presence of adsorption layers.[38] However, the qualitative friction properties, i.e., the behavior of the lateral forces on the C_{60} layers compared with the lateral forces on the GeS substrate, were highly reproducible.

The samples presented in Figs. 4 and 5 were produced using a home-built evaporation cell, as already mentioned in the experimental part. The evaporation time for the sample shown in Fig. 4 was 11 min; its nominal thickness is estimated to about 2 ML. In the LEED pattern, which was obtained after deposition of the C_{60} molecules, some characteristic spots of the GeS substrate were still visible. These spots were reported to disappear at a coverage above ≈ 3 ML.[39] The scanned surface area is 5×5 μm^2. The corresponding friction image is not displayed because it was featureless. Hence it follows that the entire substrate surface is covered by C_{60} molecules. Two types of steps are visible: Sharp, straight steps, which are considered to be due to substrate surface steps being 5 or 10 Å high, and more diffuse steps, which are interpreted as surface steps of the C_{60} layers. Certain areas of the sample surface are densely overgrown with small "islands" of 1–4-ML height and 10–100-nm diameter.

The sample shown in Fig. 5 was sublimed with the same parameters as the sample in Fig. 4, except for a longer evaporation time of 60 min. Consequently, the estimated layer thickness is 11 ML. In Fig. 5(a), a surface area of 5×5 μm^2 and in Fig. 5(b), a surface area of 3.6×3.6 μm^2 was mapped. The corresponding friction images were again featureless and are, therefore, not displayed here. On both images, structures of roughly triangular shape are observed, reflecting the sixfold symmetry of the {111} surface of the fcc lattice of the C_{60} molecules. Two different types of triangular islands can be distinguished: islands with one of their corners pointing downwards in Fig. 5 (type I islands), and islands (type II) rotated by 180° relative to these type I islands. It is remarkable that islands coalesce with other islands of the same type to form rather complicated structures, whereas islands of different type are always separated by a groove. These grooves are 50–140 nm wide and usually one ML deep. Sometimes, a second groove of 1 ML depth, but only 10–50-nm width can be observed at the bottom of the main groove. Some areas of the sample are, similar to the 2-ML film, covered with arbitrarily shaped small "islands" of about 10–150-nm diameter and 1–4-ML height, the majority of them being 2 or 3 ML high. The areas with these small islands are clearly separated from the triangular island areas.

IV. DISCUSSION

The results presented above show varying growth behavior on the samples investigated. On most specimens, the obtained data is in agreement with a layer-by-layer (Frank–van der Merwe) growth found for C_{60} on GeS(001) when evaporated at substrate temperatures between 180 °C and 200 °C,[18] whereas the growth mode for the 1.2-ML sample is significantly different. The observed film morphologies and the supposed reason for the change in growth behavior will be discussed in the following.

The 0.7-ML film presented in Fig. 1 shows only 1 ML high surface steps. As mentioned above, growth of a second C_{60} layer was not observed at any surface spot investigated. The individual islands have diameters of about 1 μm, which is quite large in comparison with the average diameter of 110 nm reported for the individual islands of a 2.4-ML film on mica[40] and the island diameter of 100–300 nm for a 3-ML film on NaCl.[15] This is in agreement with the layer-by-layer-type growth mode postulated above. The round shape of the islands is contrary to the faceted growth of the C_{60} islands found in Ref. 15. However, it is known that silver, e.g., which also has an fcc structure, can show a similar behavior if it grows homoepitaxial on Ag(111).[41]

The results obtained for the 0.95-, the 2-, and the 11-ML samples also confirm a layer-by-layer growth model.

Except for small holes, the whole substrate surface of the 0.95-ML film is covered by a monomolecular film of C_{60} molecules, thus excluding island growth (Volmer-Weber). On the 2- and the 11-ML sample, small, 1–4 ML high islands occur, but merely locally. If the "islands" would have been already formed during the evaporation process in the vapor phase or even in the evaporation cell itself, they should be equally distributed over the sample surface like the "clusters" on the 0.7-ML sample. Moreover, the clusters are easily movable, whereas the "islands," which were observed also on several other samples investigated in this study, but not discussed here, stay at defined spots. Most regions do not exhibit island formation and show the appearance of pure layer-by-layer growth. Assuming a formation of the islands during the growth process, it follows that two different growth modes are established in close vicinity of each other. Probably, a better explanation for the occurrence of the small islands is, therefore, an oxidation of the film (or another reaction of the film with the humid air) when it is taken out of the vacuum chamber. Oxidation, which is under ambient conditions and at room temperature known to be due to a reaction of C_{60} molecules with ozone[42] or with O_2 when stimulated by visible light,[43] would only occur at certain spots, depending, e.g., on the defect density. Thus, the growth mode of the film in UHV would be of pure layer-by-layer (Frank–van der Merwe) type. Oxidation is also considered to be the origin of the small, easily movable clusters observed in Figs. 1 and 2. This assumption is supported by the observation that on the sample displayed in Fig. 4, the density of the clusters rose significantly on a time scale of some days.

In the case of the 1.2-ML sample, the growth mode has changed to a nonideal layer-by-layer type. The islands have a dendritic shape and the individual branches are not correlated with the orientation of the substrate. Second- and even third-layer growth started before the first layer has been completed. Similar dendritic shapes were also observed for Au on Ru(0001) (Ref. 44) or Pt on Pt(111),[45,46] where the shapes of the islands were explained by a two-dimensional diffusion-limited growth mechanism. According to this mechanism, lower sample temperatures hinder the diffusion of the C_{60} molecules along the step edges of the C_{60} islands; the individual C_{60} molecules are likely to stick to the position where they first hit the step edge. Second- and third-layer growth starts, because the reduced energy of the C_{60} molecules at those temperatures is too low to cross the potential barrier at the island edge (often called the "Schwoebel barrier").[41,46]

The influence of temperature on the growth mode is supported by observations already published in Refs. 18, 27, and 39. In these studies, a quite strong temperature dependence of the LEED signal was found. For substrate temperatures significantly below 180 °C during deposition, a sharp LEED signal was not observed, contrary to the temperature regime between 180 °C and 200 °C, where sharp LEED patterns have been reported. The growth mode was found to be of the layer-by-layer (Frank–van der Merwe) type, using x-ray photoemission spectroscopy (XPS) and reflection x-ray scattering. For annealing temperatures from 200 °C to 220 °C, the C_{60} molecules from the second and higher layers evaporate, which indicates that the substrate-molecule interaction at these temperatures is higher than the intermolecular interaction. This was confirmed by additional XPS investigations. Temperatures higher than 220 °C cause a complete evaporation of all C_{60} molecules from the substrate.

All C_{60} samples investigated in this study showed a sharp LEED pattern of the {111} surface of the close-packed lattice of the C_{60} molecules. Thus, the substrate temperatures during evaporation did not differ very much from the favorable temperature regime ranging from 180 °C to 200 °C. If a mechanism similar to the one described above for Au on Ru(0001) and Pt on Pt(111) is assumed for the dendritic growth in the present case, it can be concluded that the 1.2-ML sample was prepared at a substrate temperature close to 180 °C, whereas the C_{60} layers of the other samples presented above were evaporated at substrate temperatures closer to 200 °C. This difference in temperature is possible since the substrate was, as already described in the experimental part, heated indirectly by means of an infrared light source, and no temperature sensor was mounted on the sample holder itself.

The last point of the present discussion is devoted to an analysis of the surface structure of the 11-ML film. As already stated above, the triangular islands which are observed on this sample can be classified into two different types: one class of islands with their corners pointing downwards in Fig. 5 and a second class with islands rotated by 180° relative to the islands of type I. It is well known that close-packed steps are energetically most stable. If a simple hard-sphere model is used (Fig. 8), it can be seen that two structurally different types of close-packed steps parallel to the ⟨110⟩ directions exist on a (111) surface of a fcc crystal. The first type is part of a small {100} microfacet and will be termed *A* step in the following [see Fig. 8(a) for illustration], the second type (*B* step) is part of a {111} microfacet [Fig. 8(b)].[47] Michely *et al.*[45] found for Pt on Pt(111) that the growth speeds of *A* and *B* steps are different, probably due to a different mobility of the adatoms along the different types of steps. These different growth speeds were temperature dependent in such a manner that at a certain temperature, the observed island shapes of the growth hills were triangular and bound by *A* steps, whereas at a higher-temperature regime, *B* steps were reported to be more stable, leading to a formation of triangular islands rotated by 180° relative to the triangular islands grown in the low-temperature regime.

The mechanism for the growth of C_{60} molecules on GeS(001) proposed here is the following: The first layer of C_{60} molecules grows epitaxially according to the structural model presented in Fig. 6 until the whole substrate surface is covered with one complete monolayer. In the subsequent growth of C_{60} on C_{60}(111), one type of the close-packed steps is energetically more stable than all other types of steps. This leads to the triangular shape of the observed islands. Since molecular resolution at the step edges was not yet obtained, it cannot be determined from the present data whether the *A*- or the *B*-type step

is the more stable one in the temperature regime between 180 °C and 200 °C. The different types of triangular islands (type I and type II) might be induced by a stacking fault: Second-layer growth starts on the first continuous monolayer of C_{60} molecules at several different nucleation sites. The location of two neighboring nucleation sites is sometimes off by half of the nearest-neighbor distance in ⟨110⟩ direction. This offset gives rise to the occurrence of a domain boundary if islands with different stacking are starting to coalesce (see Fig. 8). If the energy of the C_{60} molecules is high enough, the stacking fault might be healed up and a second complete monolayer is formed. If not, two different types of domains are formed. Assuming the *A*-type steps to be more stable, this leads to the formation of triangular-shaped islands as sketched in Fig. (8)(a); otherwise, if the *B*-type steps are energetically more favorable, islands according to Fig. 8(b) grow. For the third layer, the nucleation sites for the C_{60} molecules, arriving from the vapor phase during the growth process, are defined by the first two layers, and no additional domains will be formed. To minimize the surface energy, islands belonging to the same type of domain like to coalesce. On the other hand, the occurrence of grain boundaries as depicted in Fig. 8 is energetically unfavorable. A reduction of the boundary energy might be realized by a reduction of the distance between the individual molecules at the boundary, inducing a stress in the lattice close to the domain boundary. Such a mechanism could explain why the area between different type of domains is filled with C_{60} molecules at a later stage of the growth process. This results in sometimes rather complicated growth structures formed by coalescence of triangular islands of the same type, whereas islands belonging to different types have quite large grooves between them.

To complete the analysis of the 11-ML film, two more aspects of the surface structure should be noted. The ob-

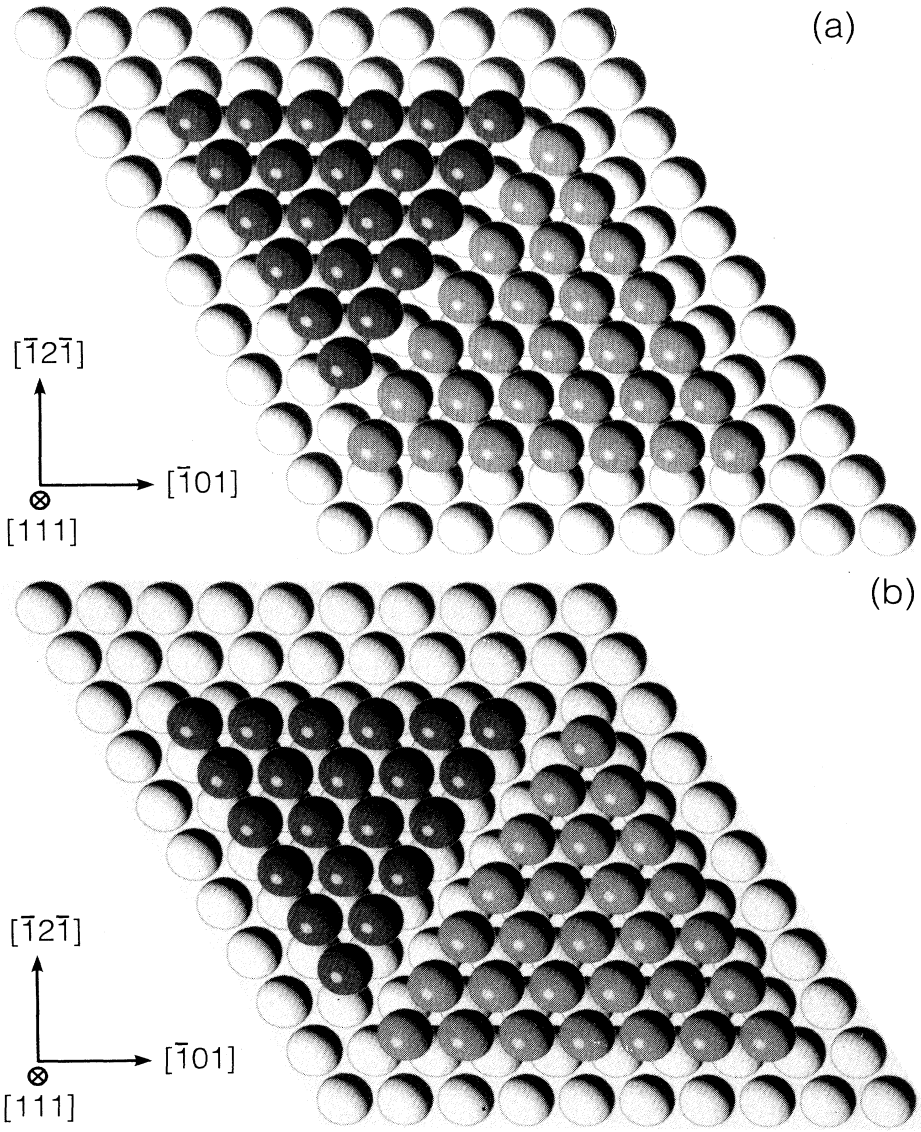

FIG. 8. (a) Triangular islands of different types, bound by *A*-type steps (see text). Different stacking of the C_{60} molecules on the first layer gives rise to the occurrence of a domain boundary. (b) is similar to (a), but with islands bound by *B*-type steps.

served angles are not precisely 60° or 120°, they vary about ±20°. Additionally, the edges of the triangles are also not really straight, but rather rough. This specific morphology might be caused by two factors. First, during the growth of the islands, the distribution of the density of the C_{60} molecules arriving from the vapor phase on the sample surface shows its steepest gradient close to the corners. Hence, the corners of the islands receive an increased supply of molecules.[48] With increasing length of the island edges, this additional supply of molecules can no longer be compensated by diffusion along the edges, leading to a self-accelerated growth of the triangle corners, as, e.g., reported in Ref. 45. Second, the rough edge structure points to a hindered diffusion along the edges during evaporation. This would fit into the scenario that is close to 200 °C, where evaporation of the second and the higher C_{60} layers starts, the mobility of the C_{60} molecules is high enough for the individual domains to be healed up and continuous layers are formed; at somewhat lower sample temperatures, however, the hindered mobility of the molecules leads to the formation of domains, which show the observed rough edge structure.

V. CONCLUSIONS

With the experiments described above, the epitaxial growth of C_{60} molecules on GeS(001) substrates under UHV conditions has been investigated by scanning force microscopy in air. Well-ordered C_{60} layers were only obtained at substrate temperatures between 180 °C and 200 °C during evaporation. In this small favorable temperature regime, thin film growth was found to be very sensitive to slight changes in temperature. The variety of growth mechanisms observed include pure layer-by-layer growth, growth with the domain formation leading to a surface structure with triangular-shaped islands, and dendritic growth according to a two-dimensional diffusion-limited growth model.

ACKNOWLEDGMENTS

We are indebted to R. L. Johnson and O. Wolter for helpful support of this work. Additionally, we thank H. Bluhm, M. Löhndorf, P. Köster, and S. H. Pan for useful discussions. Financial support from the Deutsche Forschungsgemeinschaft (Grant No. WI 1277/2-1) is gratefully acknowledged.

[1]H. W. Kroto, J. R. Heath, S. C. O'Brian, R. F. Curl, and R. E. Smalley, Nature **318**, 162 (1985).
[2]W. Krätschmer, L. D. Lamb, K. Fostiropoulos, and D. R. Huffman, Nature **347**, 354 (1990).
[3]R. L. Meng, D. Ramirez, X. Jiang, P. C. Chow, C. Diaz, K. Matsuishi, S. C. Moss, P. H. Hor, and C. W. Chu, Appl. Phys. Lett. **59**, 3402 (1991).
[4]M. Haluška, H. Kuzmany, M. Vyboronov, P. Rogl, and P. Fejdi, Appl. Phys. A **56**, 161 (1993).
[5]J. E. Rowe, P. Rudolf, L. H. Tjeng, R. A. Malic, G. Meigs, C. T. Chen, and E. W. Plummer, Int. J. Mod. Phys. B **6**, 325 (1992).
[6]E. I. Altman and R. J. Colten, Surf. Sci. **279**, 49 (1992).
[7]E. I. Altman and R. J. Colten, Phys. Rev. B **48**, 18 244 (1993).
[8]J. K. Gimzewski, S. Modesti, C. Gerber, and R. R. Schlittler, Chem. Phys. Lett. **213**, 401 (1992).
[9]Y. Z. Li, J. C. Patrin, M. Chander, J. H. Weaver, L. P. F. Chibante, and R. E. Smalley, Science **252**, 547 (1991).
[10]Y. Z. Li, M. Chander, J. C. Patrin, J. H. Weaver, L. P. F. Chibante, and R. E. Smalley, Science **253**, 429 (1991).
[11]X.-D. Wang, T. Hashizume, H. Shinohara, Y. Saito, Y. Nishina, and T. Sakurai, Jpn. J. Appl. Phys. **31**, L983 (1992).
[12]W. M. Tong, D. A. Ohlberg, H. K. You, R. S. Williams, S. J. Anz, M. M. Alvarez, R. L. Whetten, Y. Rubin, and F. N. Diederich, J. Phys. Chem. **95**, 4709 (1991).
[13]T. Ichihashi, K. Tanigaki, T. W. Ebbesen, S. Kuroshima, and S. Iijima, Chem. Phys. Lett. **190**, 179 (1992).
[14]K. Tanigaki, S. Kuroshima, J. Fujita, and T. W. Ebbesen, Appl. Phys. Lett. **63**, 2351 (1993).
[15]R. Lüthi, H. Haefke, E. Meyer, L. Howald, H.-P. Lang, G. Gerth, and H.-J. Güntherodt, Z. Phys. B **95**, 1 (1994).
[16]M. Sakurai, H. Tada, K. Saiki, and A. Koma, Jpn. J. Appl. Phys. **30**, L1892 (1991).
[17]A. Manivannan, H. Hoshi, L. A. Nagahara, Y. Mori, Y. Maruyama, K. Kikuchi, Y. Achiba, and A. Fujishima, Jpn. J. Appl. Phys. **31**, 3680 (1992).
[18]G. Gensterblum, K. Hevesi, B.-Y. Han, L.-M. Yu, J.-J. Pireaux, P. A. Thiry, R. Caudano, A.-A. Lucas, D. Bernaerts, S. Amelinckx, G. Van Tendeloo, G. Bendele, T. Buslaps, R. L. Johnson, M. Foss, R. Feidenhans'l, and G. Le Lay, Phys. Rev. B **50**, 11 981 (1994).
[19]W. Allers, U. D. Schwarz, G. Gensterblum, and R. Wiesendanger, Appl. Phys. A **59**, 11 (1994).
[20]E. Meyer, R. Overney, D. Brodbeck, L. Howald, R. Lüthi, J. Frommer, and H.-J. Güntherodt, Phys. Rev. Lett. **69**, 1777 (1992).
[21]P. J. Blau and C. E. Haberlin, Thin Solid Films **219**, 129 (1992).
[22]B. Bhushan, B. K. Gupta, G. W. Van Cleef, C. Capp, and J. C. Coe, Appl. Phys. Lett. **62**, 3253 (1993).
[23]J. Ruan and B. Bhushan, J. Mater. Res. **8**, 3019 (1993).
[24]B. Bhushan and B. K. Gupta, J. Appl. Phys. **75**, 6156 (1994).
[25]T. Thundat, R. J. Warmack, D. Ding, and R. N. Compton, Appl. Phys. Lett. **63**, 891 (1993).
[26]R. Lüthi, E. Meyer, H. Haefke, L. Howald, W. Gutmannsbauer, and H.-J. Güntherodt, Science **266**, 1979 (1994).
[27]J.-M. Themlin, S. Bouzidi, F. Coletti, J.-M. Debever, G. Gensterblum, L.-M. Yu, J.-J. Pireaux, and P. A. Thiry, Phys. Rev. B **46**, 15 602 (1992).
[28]Nanoscope III, Digital Instruments, Santa Barbara, CA.
[29]G. Meyer and N. M. Amer, Appl. Phys. Lett. **53**, 1045 (1988).
[30]S. Alexander, L.Hellemans, O. Marti, J. Schneir, V. Elings, P. K. Hansma, M. Longmire, and J. Gurley, J. Appl. Phys. **65**, 164 (1989).
[31]O. Marti, J. Colchero, and J. Mlynek, Nanotechnology **1**, 141 (1990).
[33]Nanosensors, Aidlingen, Germany.
[34]T. Grandke and L. Ley, Phys. Rev. B **16**, 832 (1977).
[35]R. Overney and E. Meyer, MRS Bull. **19** (3), 26 (1993).
[36]S. Grafström, M. Neitzert, T. Hagen, J. Ackermann, R. Neumann, O. Probst, and W. Wörtge, Nanotechnology **4**, 143 (1993).

[37]U. D. Schwarz, W. Allers, G. Gensterblum, and R. Wiesendanger (unpublished).
[38]M. Binggeli and C. M. Mate, Appl. Phys. Lett. **65**, 415 (1994).
[39]G. Gensterblum, L.-M. Yu, J.-J. Pireaux, P. A. Thiry, R. Caudano, J.-M. Themlin, S. Bouzidi, F. Coletti, and J.-M. Debever, Appl. Phys. A **56**, 175 (1993).
[40]H.-G. Busmann, R. Hiss, H. Gaber, and I. V. Hertel, Surf. Sci. **289**, 381 (1993).
[41]J. Tersoff, A. W. Denier van der Gon, and R. M. Tromp, Phys. Rev. Lett. **72**, 266 (1994).
[42]L. P. Felipe and D. Heymann, Geochim. Cosmochim. Acta **57**, 1879 (1993).
[43]A. M. Rao, K.-A. Wang, J. M. Holden, Y. Wang, P. Zhou, P. C. Eklund, C. C. Eloi, and J. D. Robertson, J. Mater. Res. **8**, 2277 (1993).
[44]R. Q. Hwang, J. Schröder, C. Günther, and R. J. Behm, Phys. Rev. Lett. **67**, 3279 (1991).
[45]T. Michely, M. Hohage, M. Bott, and G. Comsa, Phys. Rev. Lett. **70**, 3943 (1993).
[46]M. Bott, T. Michely, and G. Comsa, Surf. Sci. **272**, 161 (1992).
[47]T. Michely and G. Comsa, Surf. Sci. **256**, 217 (1991).
[48]W. W. Mullins and R. F. Sekerka, J. Appl. Phys. **34**, 323 (1963).

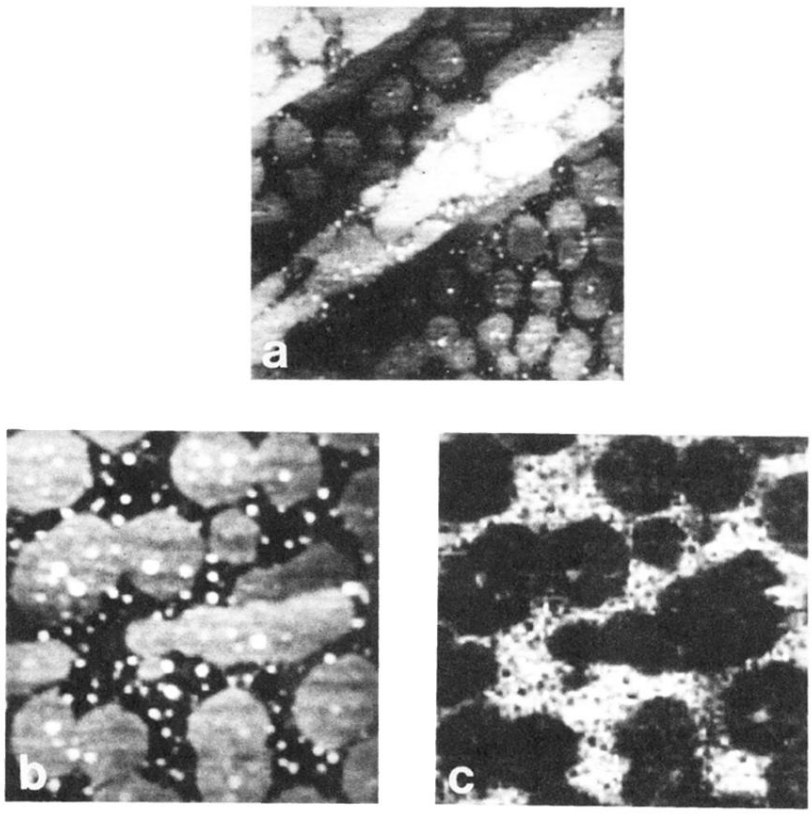

FIG. 1. (a) Force micrograph of a 0.7-ML film. The scanned area was $9.3 \times 9.3\ \mu m^2$. The observed islands are 1 nm high, corresponding to 1-ML C_{60}. The average diameter of an island is around 1 μm. (b) Topography and (c) lateral force map of a smaller surface area on the same film ($4 \times 4\ \mu m^2$). The contrast in the lateral force map indicates lower friction on the C_{60} islands.

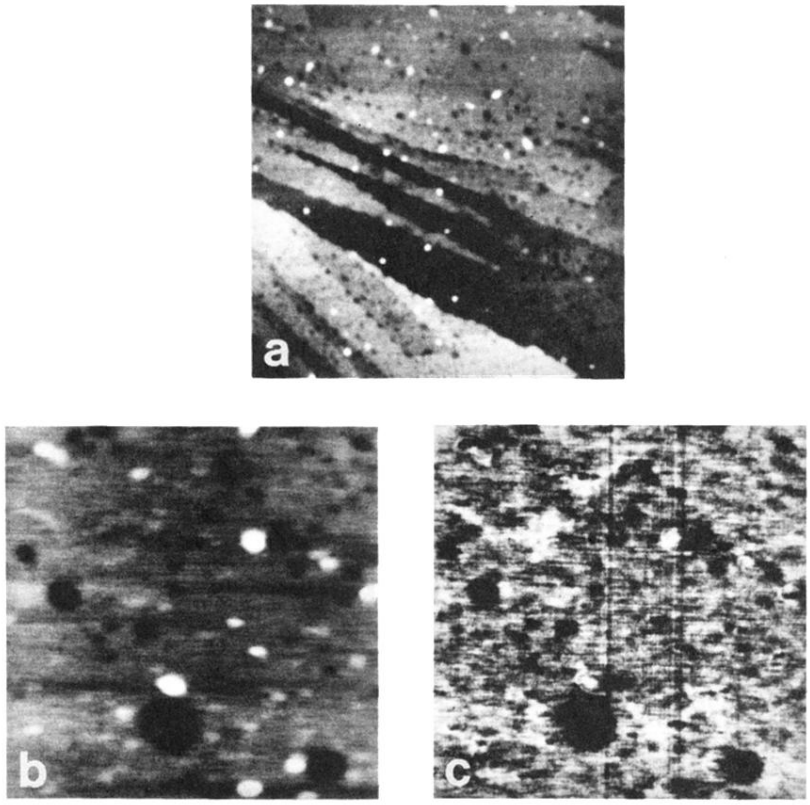

FIG. 2. (a) Large-scale scan (12.5×12.5 μm^2) of a 0.95-ML film. Small holes are observed. The step structure is induced by the cleavage steps of the underlying substrate. (b) Zoom of (a) for a closer examination of the holes. These holes are found to be 1-nm deep and flat at the bottom. The corresponding lateral force image (c) exhibits a different friction at the bottom of the holes compared with the surface of the film. The reversed contrast [cf. Fig. 1(c)] is explained in the text.

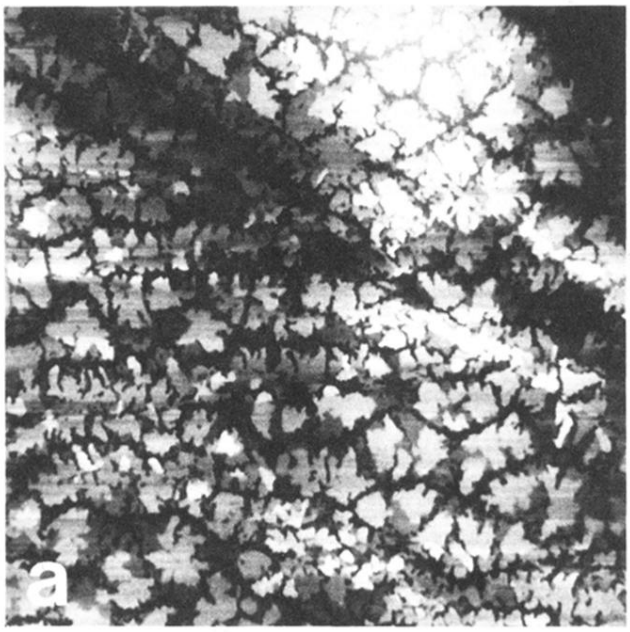

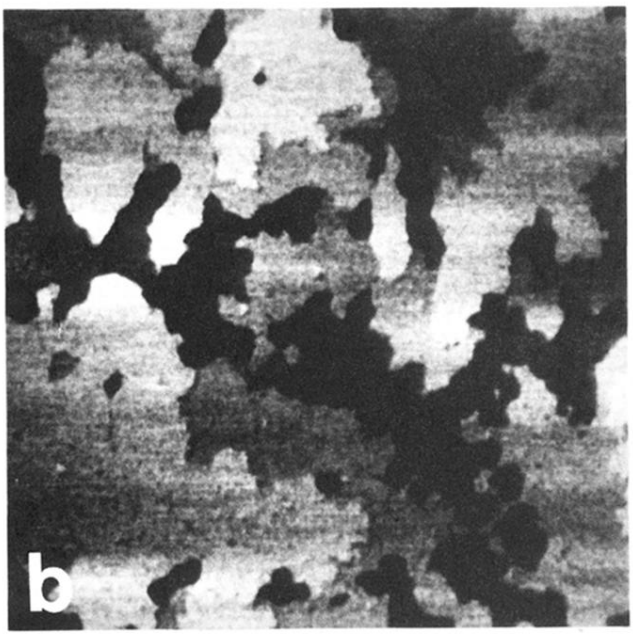

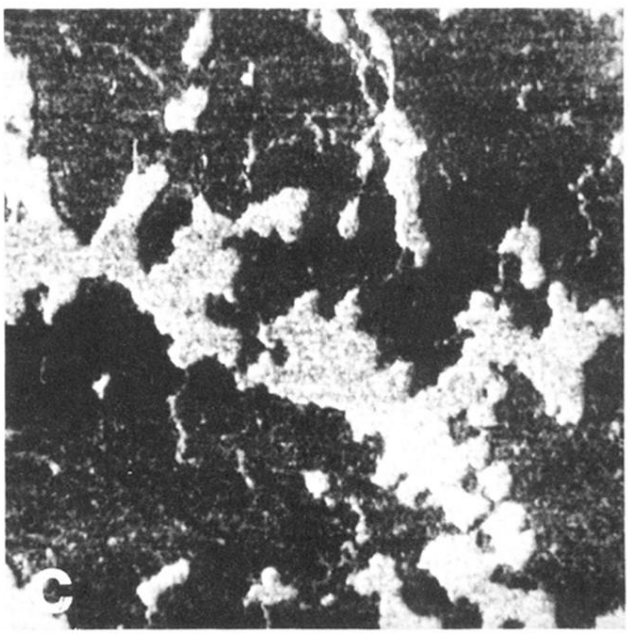

FIG. 3. Large-scale scan [(a) $10\times10\ \mu m^2$] and higher magnification image [(b) $1.5\times1.5\ \mu m^2$] of a film with 1.2-ML nominal coverage. The individual islands have about the same diameter as the islands in Fig. 1, but exhibit a dendritic shape. Second and even third monolayer growth starts before the first monolayer has been completed. The individual monolayers are well resolved. (c) Lateral force map of the surface area displayed in (b). The clear contrast allows an easy distinction between substrate and C_{60} layers.

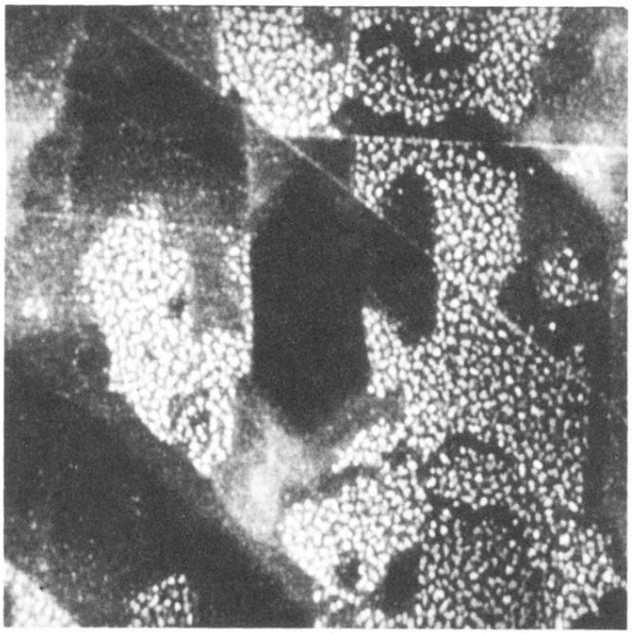

FIG. 4. SFM micrograph (5×5 μm^2) of a sample with $\approx$2-ML coverage. The corresponding lateral force map showed no contrast, indicating that the whole substrate is covered with at least one layer of C_{60}.

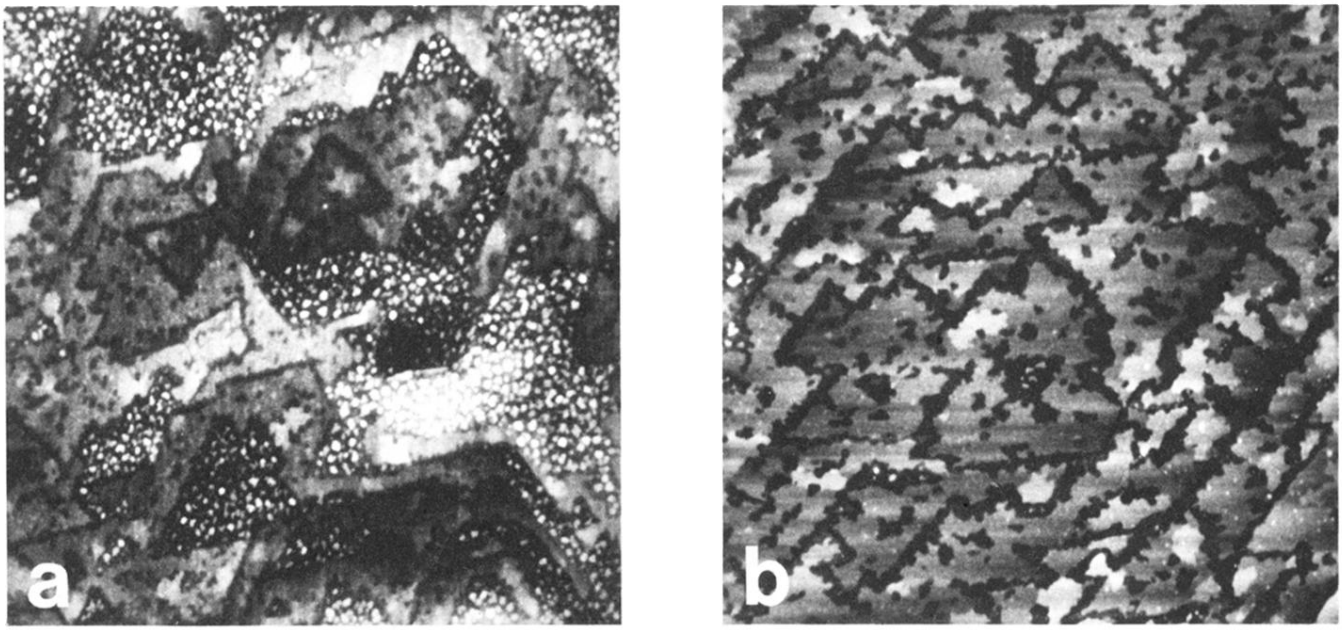

FIG. 5. Force micrographs of two different surface areas on a sample with about 11-ML coverage. The scanned areas are (a) 5×5 μm^2 and (b) 3.6×3.6 μm^2. The triangular-shaped islands, reflecting the sixfold symmetry of the $C_{60}\{111\}$ surface, are separated by grooves of 1-ML depth and 50–140-nm width. A mechanism which could explain the observed surface structure is proposed in the discussion.

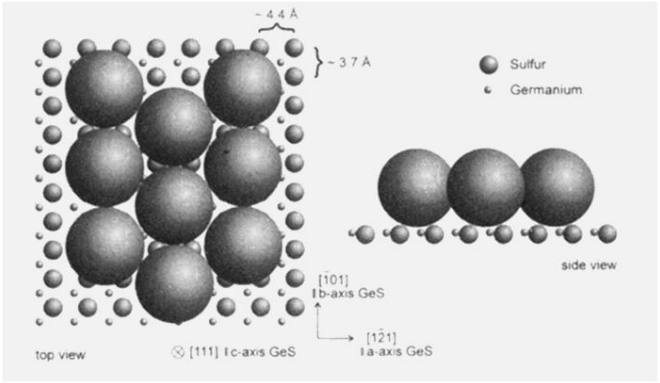

FIG. 6. Structural model for C_{60} molecules on GeS(001). Due to the anisotropy of the *a* and *b* axes of the GeS crystal and the different radii of the sulfur and the germanium ions, parallel rows in the *b* direction with 4.4-Å distance are formed on the GeS(001) surface. This is nearly half of the interlayer distance of two {111} layers in the C_{60} bulk crystal. If every second row is filled, the nearest-neighbor distance of two C_{60} molecules fits well to the 10.02-Å bulk value. Therefore, large grains with low internal stress can be formed.

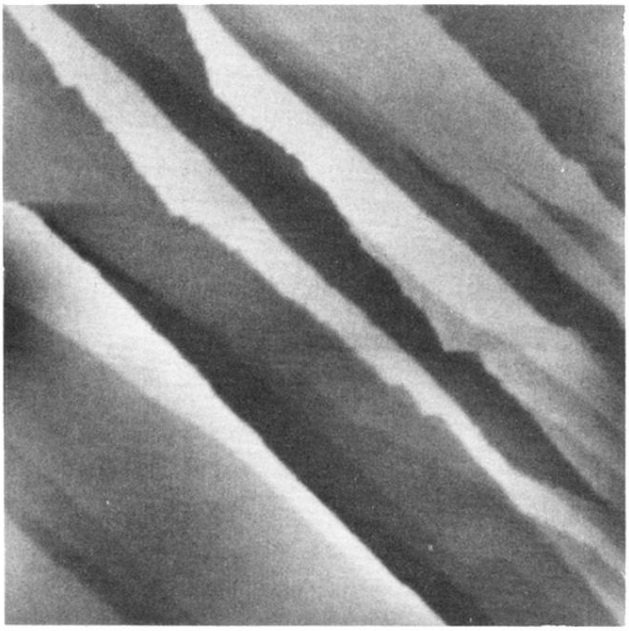

FIG. 7. SFM micrograph of freshly cleaved GeS(001). The image is dominated by large, atomically flat terraces, which are separated by steps of half of the *c*-axis lattice-constant height (5.3 Å) and multiples of this value. The scanned surface area is $50 \times 50\ \mu m^2$.

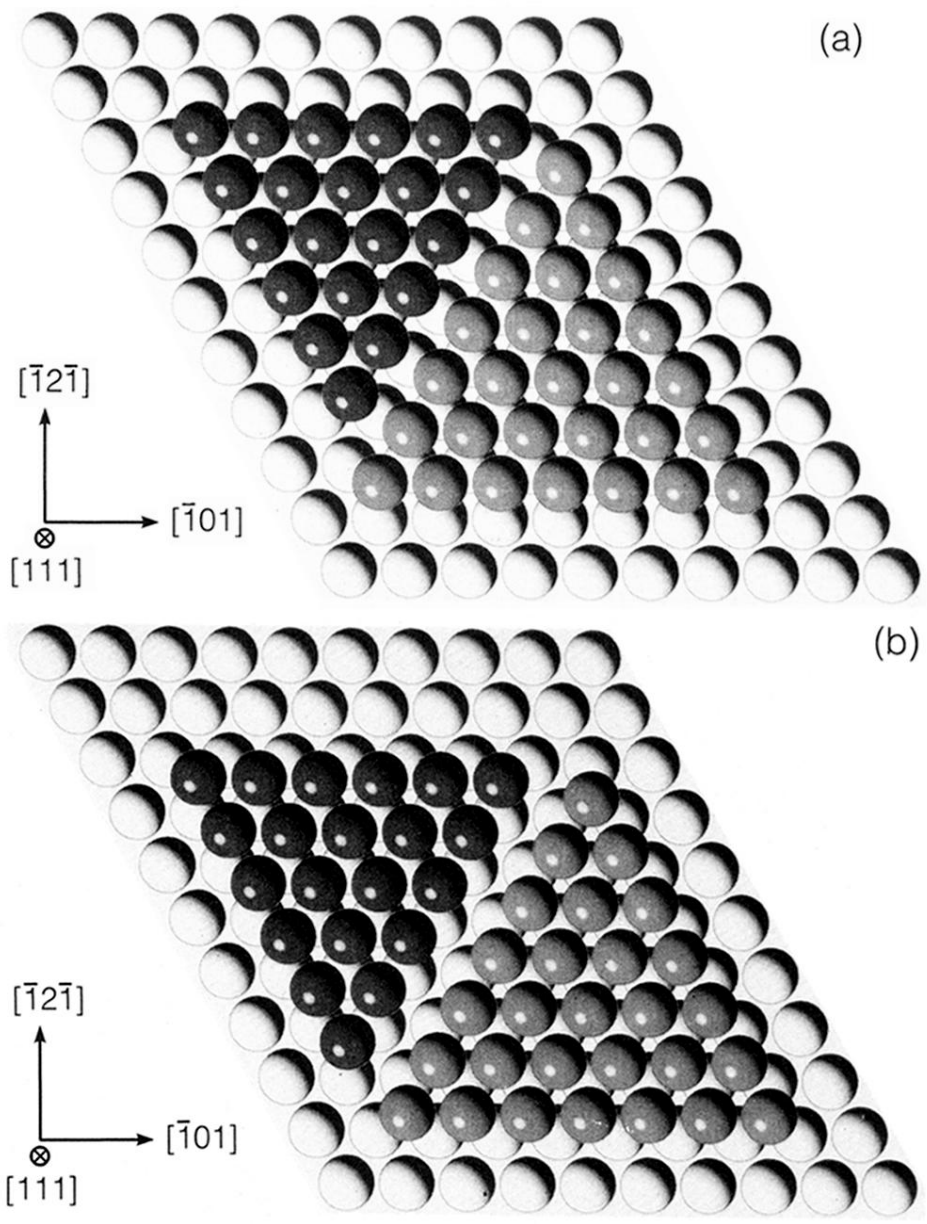

FIG. 8. (a) Triangular islands of different types, bound by *A*-type steps (see text). Different stacking of the C_{60} molecules on the first layer gives rise to the occurrence of a domain boundary. (b) is similar to (a), but with islands bound by *B*-type steps.